

This is an Open Access document downloaded from ORCA, Cardiff University's institutional repository: <https://orca.cardiff.ac.uk/id/eprint/131837/>

This is the author's version of a work that was submitted to / accepted for publication.

Citation for final published version:

Delarmelina, Maicon , Quesne, Matthew G. and Catlow, C. Richard A. 2020. Modelling the bulk properties of ambient pressure polymorphs of zirconia. *Physical Chemistry Chemical Physics* 22 (12) , pp. 6660-6676. 10.1039/D0CP00032A

Publishers page: <http://dx.doi.org/10.1039/D0CP00032A>



Please note:

Changes made as a result of publishing processes such as copy-editing, formatting and page numbers may not be reflected in this version. For the definitive version of this publication, please refer to the published source. You are advised to consult the publisher's version if you wish to cite this paper.

This version is being made available in accordance with publisher policies. See <http://orca.cf.ac.uk/policies.html> for usage policies. Copyright and moral rights for publications made available in ORCA are retained by the copyright holders.



Modelling the bulk properties of ambient pressure polymorphs of zirconia†

Macon Delarmelina, *^{ab} Matthew G. Quesne ^{ab} and C. Richard A. Catlow^{ab}

We report a detailed survey of the calculated bulk properties of zirconia using GGA and meta-GGA functionals (PBE, PBEsol, RPBE, and TPSS), dispersion (Grimme's D2 and D3 approach), and on-site Coulomb repulsion correction ($U = 2\text{--}8$ eV). Structural, elastic, mechanical, and dielectric properties, as well as energetics, electronic structure, and phonon dispersion curves were computed and compared to previous investigations to identify the best DFT approach for a consistent *in silico* description of zirconia polymorphs. In general, inclusion of dispersion corrections led to only small changes in the calculated properties, whereas DFT+ U ($U = 2$ or 4 eV) reduced the deviations of calculated properties from the experimental results, although deterioration of the structure and relative stabilities may be observed in some cases. Standard PBEsol, RPBE+ U , and PBE+ U were the best methodologies for a simultaneous description of the three polymorphs of ZrO_2 . RPBE+ U , however, was the only functional to conserve the distinct structures and stabilities of *c*-, *t*-, and *m*- ZrO_2 when $U = 4$ eV was used, resulting in the best *in silico* replication of the band gaps of ZrO_2 , whilst outperforming the other methodologies in the description of elastic, mechanical, and dielectric properties of this material. Overall, these results provide insight into the most appropriate DFT methodology for *in silico* investigations of ZrO_2 , and show that simultaneous description of all three ambient pressure zirconia polymorphs by DFT techniques with acceptable levels of accuracy can be achieved only when the correct choice of methodology is applied.

Introduction

Zirconia (ZrO_2) is an important ceramic material, which has found numerous technological applications due to its thermal, dielectric, mechanical, chemical, and biocompatibility properties. The wide range of applications of ZrO_2 include: as a ceramics toughening agent,¹ thermal barrier coating,² gas sensor,³ solid oxide fuel cell electrode,⁴ and in surface passivation.⁵ At ambient pressure ZrO_2 can exist in three distinct phases: monoclinic (*m*- ZrO_2 , space group $\text{P}2_1/\text{c}$), tetragonal (*t*- ZrO_2 , $\text{P}4_2/\text{nmc}$), and cubic (*c*- ZrO_2 , $\text{Fm}3\text{m}$). *m*- ZrO_2 is thermodynamically stable at ambient temperatures, whereas *t*- ZrO_2 and *c*- ZrO_2 are obtained at temperatures ranging between $1180\text{--}2370$ °C and $2370\text{--}2600$ °C, respectively.^{6–8} Three high pressure orthorhombic polymorphs (ortho-I – Pbca , ortho-II – Pnma , and ortho-III – $\text{Pca}2_1$) are also known; however they are not included in the scope of this study.⁹

Despite its technological importance, experimental investigation of ZrO_2 can be extremely challenging at high pressure

and temperature conditions. Usually, modification of the chemical structure (doping) is required to stabilize some polymorphs at lower temperatures and allow their characterization.¹⁰ For these reasons, the investigation of pure and doped zirconia can be greatly assisted by computational approaches, which can provide information on bulk and surface properties for comparison to experimental studies. DFT calculations are playing a major role in the study of both zirconia and other oxides, either for characterisation of known systems, or by acting as a predictive tool for the design of new materials. However, due to the large number of existing DFT functionals and other associated widely used approximations,^{7–9,11–41} there is a need to evaluate the most appropriate DFT method(s) for describing both bulk and surface properties of ZrO_2 .

A wide range of different methods have been used in previous work to predict bulk properties and catalytic activity of ZrO_2 .^{8,11–34,41} Moreover, additional corrections (e.g. dispersion and Hubbard corrections) are often introduced when, for instance, more accurate descriptions of band gaps and band structures are required, or when the description of adsorbates on the surface is investigated.^{7,9,35–40} Nevertheless, a *a priori* determination of the best methodology for a system of interest is a daunting task, especially when full experimental characterisation of the investigated material or previous thorough comparison of alternative computational methods is not available.

^a School of Chemistry, Cardiff University, Main Building, Park Place, Cardiff CF10 3AT, UK. E-mail: DelarmelinaM@cardiff.ac.uk

^b UK Catalysis Hub, Research Complex at Harwell, STFC Rutherford Appleton Laboratory, Didcot, Oxfordshire OX11 0FA, UK

Furthermore, when investigating catalytic activity on different phases of the same compound, the selection of the best computational approach can be an even more complex question, as the same theoretical methods are required to describe simultaneously all polymorphs with similar accuracy and efficiency.

In this study we will present a detailed comparative study of the different DFT approaches for the description of bulk properties of ambient pressure ZrO_2 . The performance of PBE-derived GGA (PBE, PBEsol and RPBE) and Meta-GGA (TPSS) functionals are thoroughly explored for their prediction of structural, elastic, mechanical, and dielectric properties, as well as energetics, electronic structure, and phonon dispersion curves. Moreover, the effect of Grimme's semiclassical dispersion corrections (D2 and D3) and Hubbard correction (U, $U = 2\text{--}8\text{ eV}$) for dealing with on-site coulomb repulsion interactions was also investigated. Our study allows us to identify and rationalise the efficiency of commonly used DFT methods for the bulk properties of ZrO_2 , and special attention is given to the simultaneous description of all ambient pressure polymorphs by equivalent methods. The results presented here provides a comprehensive survey of the properties of this widely investigated material and will aid all types of *in silico* investigations using ZrO_2 polymorphs by identifying the pitfalls in such methodologies that can lead to unreliable results. In the case of the lattice dynamical calculations, our results are predictive as no detailed experimental study has been reported.⁴² More generally, our survey will provide insight into the most appropriate methods for the description of bulk and surface properties of ZrO_2 and of its reactivity.

Methodology

All calculations were performed using the Vienna *ab initio* simulation package (VASP) within the framework of periodic density functional theory. Four distinct DFT functionals were investigated (PBE,⁴³ PBEsol,^{44,45} RPBE,⁴⁶ and TPSS⁴⁷), along-side the inclusion of the effect of long-range interactions using Grimme's D2 and D3 semiclassical dispersion methods,^{48,49} as well as on-site Coulomb repulsive interaction (U) for d orbitals of Zr, with U values ranging between 2–8 eV. The electron–ionic core interaction was represented by the projector-augmented-wave (PAW) potentials and the selected cutoff energy was selected after extensive benchmarking and set to 550 eV (see Fig. S1–S3, ESI†). The $\text{Zr } 4s^2 4p^6 4d^2 5s^2$ and $\text{O } 2s^2 2p^4$ orbitals were explicitly included as valence electrons. Brillouin zone sampling was performed by using the Monkhorst–Pack scheme with a k-point grid of 5 5 5 together with a Gaussian smearing broadening of 0.01 eV. A conjugate-gradient algorithm is used to relax and optimise lattice constants and atomic coordinates. Forces were set as converged at $10^{-3}\text{ eV \AA}^{-1}$.

Elastic constants were calculated by the finite difference method, in which the Hessian matrix is determined by the symmetry inequivalent displacements of each ion in the direction of each Cartesian coordinate. From the Hessian matrix, forces and elastic constants (c_{ij}) were determined. Bulk moduli values were calculated from the elastic constants using the

general equation in Voigt's approximation (eqn (1)), in which for the cubic phase $c_{11} = c_{22} = c_{33}$ and $c_{12} = c_{23} = c_{31}$, and for the tetragonal phase $c_{11} = c_{22}$ and $c_{23} = c_{31}$ were assigned.

$$B_V = \frac{1}{9} (c_{11} + c_{22} + c_{33}) + \frac{2}{9} (c_{12} + c_{23} + c_{31}) \quad (1)$$

The electronic contribution e^N to the dielectric constant ϵ was calculated by linear response, whereas the ionic contributions e^{Ion} were calculated by finite difference method. Both contributions were determined by the average of the dielectric tensors obtained for each contribution (eqn (2) and (3)), whereas the total dielectric constant was calculated by the sum of both contributions (eqn (4)). For the c- ZrO_2 , $\epsilon_{11} = \epsilon_{22} = \epsilon_{33}$. For t- ZrO_2 , $\epsilon_{11} = \epsilon_{22} \neq \epsilon_{33}$. For m- ZrO_2 , $\epsilon_{11} \neq \epsilon_{22} \neq \epsilon_{33}$.

$$\epsilon^N = \frac{1}{3} (\epsilon_{11}^N + \epsilon_{22}^N + \epsilon_{33}^N) \quad (2)$$

$$\epsilon^{\text{Ion}} = \frac{1}{3} (\epsilon_{11}^{\text{Ion}} + \epsilon_{22}^{\text{Ion}} + \epsilon_{33}^{\text{Ion}}) \quad (3)$$

$$\epsilon = \epsilon^N + \epsilon^{\text{Ion}} \quad (4)$$

Band structures were obtained for the three phases along the following high symmetry path: G–X–W–K–G–L–U–W–L–K|U–X for the c- ZrO_2 , G–X–M–G–Z–R–A–Z|X–R|M–A for t- ZrO_2 , and Z–G–Y–A–B–D–E–C for m- ZrO_2 . Phonon dispersion curves were obtained by a standard approach using the Phonopy code.⁵⁰ The optimised unit cells were used to construct supercells of each system, with supercells of dimensions 3 3 3.

Previous theoretical investigation of zirconia have used a wide range of different methods to predict ZrO_2 properties, mainly applying LDA and GGA (e.g. PW91, PBE, PBEsol and RPBE) functionals for describing bulk properties and reactivity.^{11–25} Moreover, GGA functionals combined with dispersion and Hubbard (U) corrections appear to be able to provide similar results as more robust approaches, but at lower computational cost.²⁶ In the latter approach, an on-site coulombic repulsion correction is introduced owing to the highly correlated d-(and f-) electrons, whereas the dispersion correction deals with the long-ranged electron correlation effect – or the van de Waals interactions – which are needed to account for non-covalent interactions and for accurate description of adsorbate–surface interaction;^{27–32} their inclusion has been shown to provide not only better relative energies of zirconia polymorphs and other similar systems, but also better structural properties.^{7,9,33–38} Fewer examples are found using Meta-GGA or hybrid functionals to study ZrO_2 properties, the latter being usually chosen for a better description of the band structures, even though they require higher computational time.^{39–41}

In the following subsections, we discuss the ability of the selected functionals (PBE, PBEsol, RPBE, and TPSS) to predict bulk properties of ZrO_2 . The GGA-PBE⁴³ is a widely used functional for solid state calculations, with known intermediate performance for the description of bulk and surface properties, although it usually leads to overestimated unit-cell parameters and underestimated adsorption energies. The PBEsol^{44,45} and

RPBE⁴⁶ functionals are PBE-based functionals modified to better describe solid properties and adsorption energies, respectively. PBEsol^{44,45} was constructed by modifying PBE to restore the gradient expansion for exchange and by fitting the exchange and correlation energy to the surface jellium, resulting in a good compromise between structure and surface energy. RPBE⁴⁶ uses a modified exchange enhancement factor ($F_x(s)$) that increases more rapidly than that of PBE in order to compensate the loss of regions of high s (reduced density gradient) at surface boundary upon adsorption, which yields better adsorption energies. Finally, TPSS⁴⁷ is a meta-GGA functional known for simultaneously improving bulk lattice constants and surface energies at only slightly higher computation cost than GGA functionals.

The effect of Grimme's semiclassical dispersion corrections (D2 and D3) and Hubbard correction (U, $U = 2-8$ eV) is additionally discussed alongside the standard functionals. Where possible, previous theoretical and experimental results will be presented in each subsection for comparison with the results obtained in the present study. Our results are organised as follows: first we discuss structural properties and relative stabilities of c-, t-, and m-ZrO₂; then their elastic properties, followed by dielectric and electronic properties; and, finally, we present our predictions of the phonon dispersion curves.

Results and discussion

a. Structural properties and relative stability

The optimised lattice parameters of c-, t-, and m-ZrO₂ obtained using the selected DFT methodologies are given in Tables 1–3. The experimental values⁵¹ are shown for comparison, as well as previously reported theoretical results obtained using LDA and GGA (PBE) functionals.^{7,14,52}

Our results using standard PBE were in all cases larger than the experimental values by less than 2.0%, in close agreement to the previously reported values.⁵³ Standard RPBE presented a similar trend, although in this case all calculated values gave larger deviations, up to 3.7%. As would be expected for PBEsol, all calculations gave smaller lattice parameters than the experimental

values, with smaller errors than those observed for PBE (less than 0.9%).⁵³ The only exception to this observation is the lattice parameter a_2 of the monoclinic phase, in which PBEsol overestimated the experimental value by approximately 0.2%. Finally, it was observed that TPSS underestimated the lattice vector of c-ZrO₂ by less than 0.1% but overestimated these values for t- and m-ZrO₂ phases by up to 1.0%.

In general, the dispersion correction resulted, as expected, in a slight contraction of the unit cell when compared to the standard functionals, in accordance with previous studies.²⁶ As a result, RPBE which had overestimated the lattice constants before, provided now smaller errors, up to 2.6%. On the other hand, PBEsol presents larger errors than before (up to 2.8%) as the already underestimated lattice vector were further reduced with addition of dispersion correction to the structure.

Inclusion of the Hubbard correction systematically led to expansion of the unit cell in all cases. Interestingly, higher values of U resulted in a distinct trend for the tetragonal phase, involving a sudden increase of the calculated lattice vector a_3 for PBE+ U (8 eV), PBEsol+ U (6 eV), and TPSS+ U (6 eV), as can be seen in Table 2. When analysing the changes in the two distinct bond length in this structure (Zr–O₁ and Zr–O₂), it is possible to observe a significant increase of Zr–O₁ (Fig. 1(a)) and short-ening of Zr–O₂ (Fig. 1(b)) as the value of U increases. For instance, t-ZrO₂ optimised at PBE and PBE+ U (8 eV) level gave Zr–O₁ bond lengths of 2.080 Å and 2.267 Å, respectively, whereas Zr–O₂ bond lengths were 2.429 Å and 2.267 Å. These values are the same as those obtained for c-ZrO₂ using PBE+ U (8 eV). Similarly, calculations using PBEsol+ U (6 eV) resulted in both Zr–O₁ and Zr–O₂ bond lengths of 2.234 Å for t-ZrO₂; the same value was obtained for c-ZrO₂. Analogous behaviour was observed for t-ZrO₂ and c-ZrO₂ optimised using RPBE+ U and TPSS+ U when $U = 6$ and 8 eV. These changes observed in the optimised structures when using values of $U = 6$ eV or higher are consistent with a phase transition between t-ZrO₂ - c-ZrO₂, where the disappearance of the distorted tetragonal structure of the eight oxygen anions around zirconium sites is observed.

Analysis of the relative energies of m-, t-, and c-ZrO₂ provided similar observations to those obtained from the structural changes. In Fig. 2, the relative energies of c- and t-ZrO₂ are plotted taking the total energy of m-ZrO₂ as zero. For all four standard functionals, the order of the relative stability of the three phases is m-ZrO₂ < t-ZrO₂ < c-ZrO₂, in agreement with the experimental results and previous theoretical studies.^{14,16,55} Similar behaviour is observed when dispersion corrections were used. The inclusion of Hubbard correction, however, reduced the energy difference between the three phases, up to the disappearance of the energy difference between t- and c-ZrO₂ for PBE+ U ($U = 6$ and 8 eV), PBEsol+ U ($U = 4, 6$, and 8 eV), RPBE+ U ($U = 6$ and 8 eV), and TPSS+ U ($U = 4, 6$, and 8 eV). Interestingly, it is also possible to observe that for PBE+ U ($U = 8$ eV), PBEsol+ U ($U = 6$ eV and 8 eV), and TPSS+ U ($U = 6$ eV and 8 eV) the cubic structure becomes more stable than the monoclinic structure, which disagrees with experiment and previous theoretical results where the U correction was not used.^{14,16,55} Additionally, the use of both D3 and U corrections in PBEsol-D3+ U ($U = 2$ eV) and TPSS-D3+ U ($U = 2$ eV)

Table 1 Lattice vector a_1 of the optimised unit cell of c-ZrO₂. Comparison with experimental⁵¹ and previous calculations (LDA⁵² and PBE⁷) are also provided. Relative errors (%) to the experimental values are given in parentheses

| | a_1 (Å) | | | |
|----------------------------|--------------|--------------|--------------|--------------|
| | PBE | PBEsol | RPBE | TPSS |
| — | 5.118 (0.15) | 5.067 (0.85) | 5.151 (0.81) | 5.105 (0.09) |
| D2 | 5.081 (0.57) | 5.032 (1.52) | 5.112 (0.04) | 5.070 (0.78) |
| D3 | 5.096 (0.28) | 5.049 (1.19) | 5.121 (0.22) | 5.084 (0.51) |
| U(2 eV) | 5.148 (0.74) | 5.098 (0.24) | 5.181 (1.40) | 5.135 (0.49) |
| U(4 eV) | 5.178 (1.33) | 5.129 (0.37) | 5.211 (1.98) | 5.164 (1.06) |
| U(6 eV) | 5.207 (1.90) | 5.159 (0.96) | 5.240 (2.55) | 5.193 (1.62) |
| U(8 eV) | 5.236 (2.46) | 5.189 (1.54) | 5.268 (3.10) | 5.221 (2.16) |
| D3+U(2 eV) | 5.127 (0.32) | 5.081 (0.57) | 5.153 (0.83) | 5.114 (0.08) |
| D3+U(4 eV) | 5.157 (0.92) | 5.112 (0.04) | 5.183 (1.43) | 5.144 (0.67) |
| Experimental ⁵¹ | | | 5.110 | |
| LDA ⁵² | | | 5.064 | |
| PBE ⁷ | | | 5.119 | |

Table 2 Lattice vectors a_1 and a_3 of the optimised unit cell of t-ZrO₂. Comparison with experimental⁵⁴ and previous calculations (LDA⁵² and PBE¹⁴) are also provided. Relative errors (%) to the experimental values are given in parentheses

| | a_1 (Å) | | | | a_3 (Å) | | | |
|----------------------------|--------------|--------------|--------------|--------------|--------------|--------------|--------------|--------------|
| | PBE | PBEsol | RPBE | TPSS | PBE | PBEsol | RPBE | TPSS |
| — | 3.623 (0.74) | 3.587 (0.26) | 3.646 (1.40) | 3.612 (0.45) | 5.280 (1.99) | 5.175 (0.04) | 5.367 (3.66) | 5.223 (0.89) |
| D2 | 3.597 (0.02) | 3.562 (0.94) | 3.620 (0.66) | 3.587 (0.24) | 5.212 (0.68) | 5.119 (1.12) | 5.287 (2.12) | 5.166 (0.21) |
| D3 | 3.607 (0.31) | 3.574 (0.61) | 3.625 (0.81) | 3.597 (0.04) | 5.238 (1.18) | 5.146 (0.61) | 5.312 (2.60) | 5.187 (0.18) |
| U(2 eV) | 3.644 (1.32) | 3.608 (0.32) | 3.668 (2.01) | 3.633 (1.03) | 5.253 (1.46) | 5.159 (0.34) | 5.330 (2.96) | 5.204 (0.52) |
| U(4 eV) | 3.664 (1.88) | 3.628 (0.88) | 3.688 (2.57) | 3.653 (1.58) | 5.230 (1.02) | 5.146 (0.61) | 5.298 (2.33) | 5.188 (0.22) |
| U(6 eV) | 3.682 (2.40) | 3.648 (1.44) | 3.707 (3.08) | 3.672 (2.11) | 5.211 (0.65) | 5.159 (0.35) | 5.271 (1.81) | 5.193 (0.31) |
| U(8 eV) | 3.702 (2.94) | 3.669 (2.02) | 3.725 (3.58) | 3.691 (2.65) | 5.235 (1.12) | 5.188 (0.22) | 5.268 (1.75) | 5.221 (0.85) |
| D3+U(2 eV) | 3.629 (0.91) | 3.595 (0.02) | 3.647 (1.43) | 3.618 (0.62) | 5.215 (0.73) | 5.132 (0.87) | 5.280 (1.98) | 5.170 (0.13) |
| D3+U(4 eV) | 3.648 (1.45) | 3.615 (0.54) | 3.668 (2.00) | 3.638 (1.17) | 5.194 (0.33) | 5.121 (1.09) | 5.252 (1.45) | 5.157 (0.39) |
| Experimental ⁵⁴ | | | 3.596 | | | | 5.177 | |
| LDA ⁵² | | | 3.583 | | | | 5.140 | |
| PBE ¹⁴ | | | 3.622 | | | | 5.284 | |

Table 3 Lattice vectors a_1 , a_2 , and a_3 of the optimised unit cell of m-ZrO₂. Comparison with experimental⁵⁶ and previous calculations (LDA⁵² and PBE¹⁴) are also provided. Relative errors (%) to the experimental values are given in parentheses

| | a_1 (Å) | | | | a_2 (Å) | | | | a_3 (Å) | | | |
|----------------------------|--------------|--------------|--------------|--------------|--------------|--------------|--------------|--------------|--------------|--------------|--------------|--------------|
| | PBE | PBEsol | RPBE | TPSS | PBE | PBEsol | RPBE | TPSS | PBE | PBEsol | RPBE | TPSS |
| — | 5.191 (0.90) | 5.130 (0.29) | 5.229 (1.64) | 5.159 (0.27) | 5.244 (0.72) | 5.216 (0.17) | 5.271 (1.24) | 5.259 (1.00) | 5.307 (1.24) | 5.224 (0.34) | 5.358 (2.21) | 5.258 (0.31) |
| D2 | 5.109 (0.71) | 5.037 (2.11) | 5.159 (0.26) | 5.061 (1.63) | 5.253 (0.88) | 5.227 (0.39) | 5.264 (1.10) | 5.268 (1.16) | 5.208 (0.65) | 5.096 (2.78) | 5.286 (0.83) | 5.124 (2.26) |
| D3 | 5.163 (0.34) | 5.101 (0.85) | 5.179 (0.65) | 5.124 (0.41) | 5.237 (0.58) | 5.213 (0.12) | 5.256 (0.95) | 5.256 (0.94) | 5.273 (0.58) | 5.191 (0.98) | 5.301 (1.12) | 5.215 (0.52) |
| U(2 eV) | 5.236 (1.77) | 5.176 (0.60) | 5.273 (2.48) | 5.204 (1.14) | 5.269 (1.18) | 5.241 (0.65) | 5.295 (1.70) | 5.283 (1.46) | 5.333 (1.73) | 5.255 (0.25) | 5.379 (2.61) | 5.287 (0.85) |
| U(4 eV) | 5.280 (2.63) | 5.223 (1.51) | 5.316 (3.33) | 5.249 (2.02) | 5.290 (1.59) | 5.262 (1.06) | 5.317 (2.11) | 5.305 (1.87) | 5.365 (2.34) | 5.292 (0.94) | 5.408 (3.17) | 5.321 (1.50) |
| U(6 eV) | 5.323 (3.47) | 5.269 (2.41) | 5.358 (4.14) | 5.293 (2.87) | 5.309 (1.96) | 5.281 (1.43) | 5.337 (2.50) | 5.324 (2.25) | 5.398 (2.98) | 5.330 (1.68) | 5.439 (3.76) | 5.356 (2.18) |
| U(8 eV) | 5.364 (4.26) | 5.315 (3.29) | 5.398 (4.91) | 5.335 (3.70) | 5.328 (2.33) | 5.297 (1.72) | 5.357 (2.89) | 5.342 (2.59) | 5.431 (3.61) | 5.371 (2.46) | 5.471 (4.36) | 5.393 (2.87) |
| D3+U(2 eV) | 5.208 (1.22) | 5.147 (0.05) | 5.224 (1.53) | 5.170 (0.48) | 5.262 (1.06) | 5.240 (0.63) | 5.282 (1.45) | 5.281 (1.42) | 5.300 (1.11) | 5.222 (0.39) | 5.326 (1.60) | 5.245 (0.05) |
| D3+U(4 eV) | 5.253 (2.09) | 5.194 (0.96) | 5.270 (2.43) | 5.215 (1.36) | 5.284 (1.48) | 5.263 (1.08) | 5.304 (1.86) | 5.304 (1.87) | 5.333 (1.73) | 5.257 (0.29) | 5.359 (2.24) | 5.278 (0.68) |
| Experimental ⁵⁶ | | | 5.145 | | | | 5.207 | | | | 5.242 | |
| LDA ⁵² | | | 5.122 | | | | 5.218 | | | | 5.280 | |
| PBE ¹⁴ | | | 5.190 | | | | 5.243 | | | | 5.379 | |

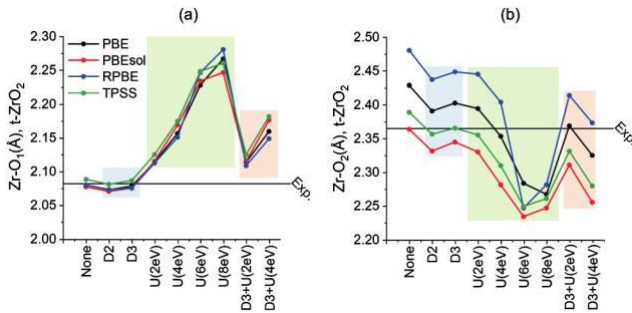


Fig. 1 Variation of Zr-O bond length in t-ZrO₂ structure from distinct DFT methodologies tested here. Zr-O₁ bond length (a) and Zr-O₂ bond length (b). Previously reported experimental⁵⁴ values are given as a solid horizontal line for comparison.

afforded an energy difference between c-ZrO₂ and t-ZrO₂ smaller than 0.07 eV, whereas these difference in energy for PBE-D3+U (U = 2 eV) and RPBE-D3+U (U = 2 eV) were calculated

as 0.135 eV and 0.238 eV, respectively. Except for RPBE-D3+U (U = 4 eV), which resulted in an energy difference of approximately 0.1 eV between c-ZrO₂ and t-ZrO₂, the combination of D3 and U = 4 eV also resulted in very small energy differences between polymorphs.

Overall, inclusion of dispersion in these calculations led to a slight reduction of the lattice vectors of ZrO₂, resulting in an improvement of those values calculated used PBE and RPBE, but in general worsening the lattice vectors calculated using PBEsol and TPSS. In this way, PBEsol and TPSS will give more accurate results for the structural parameters of zirconia if additional dispersion correction is not used. When inclusion of dispersion corrections is necessary for the investigated property, PBE and RPBE appear to be the best options amongst the functionals investigated here. As detailed before, the effect of dispersion over the relative energies was not significant. Hubbard corrections, on the other hand, resulted in significant reduction of the energy differences among the polymorphs, as

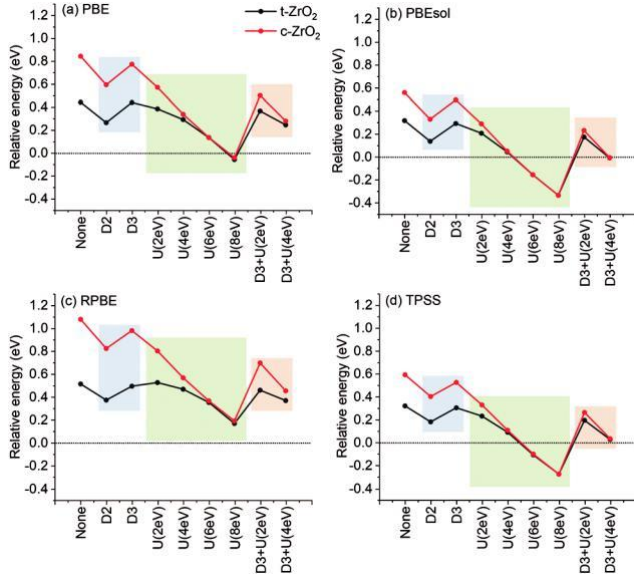


Fig. 2 Relative energy of bulk t- and c-ZrO₂ obtained for each evaluated methodology and calculated by taking the total energy of m-ZrO₂ as zero in each case (see Table S1, ESI†).

well as in larger effects over the structural properties calculated here, systematically leading to increase of the calculated lattice vectors and of the relative errors. Additionally, these results show that values of $U = 6$ eV or larger should be avoided for calculations using zirconia, as t-ZrO₂ -c-ZrO₂ phase transition and/or inversion of stability between c-ZrO₂ and m-ZrO₂ can be observed. Higher values of U may also result in the deterioration of other intrinsic bulk properties of the system without large improvements in calculated band gaps, as will be discussed in the next subsections. Interestingly, when a U value of 4 eV was used, RPBE was the only functional to conserve the structure of t-ZrO₂ and a significant energy difference between this phase and c-ZrO₂, whilst also describing m-ZrO₂ as the most stable phase. The combination of both D3 and U with RPBE also led to a good compromise between the inclusion of these additional corrections and the description of zirconia structures, presenting relative errors smaller than 2.4% for all cases investigated here.

b. Elastic properties

The calculated inequivalent elastic components c_{ij} of m-, t-, and c-ZrO₂ are shown in Fig. 3–5 along with previously reported experimental and theoretical values. The experimental values were obtained by X-ray diffraction (XRD),⁵⁷ neutron diffraction,⁵⁸ and Brillouin scattering.⁵⁹ The theoretical values used for comparison were obtained using four distinct approaches: (i) Local Density Approximation functional (LDA),⁵² (ii) finite-differences method with Generalized Gradient Approximation functional (GGA-PBE),¹⁴ (iii) finite-differences method with Generalized Gradient Approximation functional with additional Hubbard Correction $U = 2$ eV (FD),⁷ and (iv) lattice dynamics method (LD).⁶⁰

For c-ZrO₂, all calculated elastic constants c_{11} , c_{44} , and c_{12} are overestimated if compared to the experimental values, as was also observed in previous calculations using FD, LDA, and GGA, the only exception being the results obtained with LD calculations (Fig. 3(a) and (c)). Despite the overestimation of computed values, they were able to preserve the ordering $c_{11} > c_{12} > c_{44}$, which is in agreement with the experimental results.⁵⁷

The elastic constants computed with standard PBE and RPBE were close to the previous theoretical values (LDA, GGA, and FD), whereas PBEsol and TPSS afforded larger elastic constants, further away from the experimental values. In general, inclusion of dispersion correction to the calculation led to an increase of the elastic constants, which is in accordance with the above mentioned trends concerning the effect of dispersion on unit cell volume. We also observe that D2 resulted in a much more significant increase of the theoretical values than D3, leading the results obtained with the former further away from the experimental values.

Inclusion of the Hubbard correction led to a systematic decrease of the calculated c_{11} when U values were increased, whereas calculated c_{44} increases with higher values of U . The variations observed for c_{12} were less significant than those calculated for c_{11} and c_{44} , which presented small variations when compared to the results obtained with the standard functionals.

Unlike c-ZrO₂, the tetragonal phase did not present any consistent trends for all methodologies. In the cases of c_{11} , c_{66} , and c_{12} (Fig. 4a, d and e), all methodologies gave overestimated

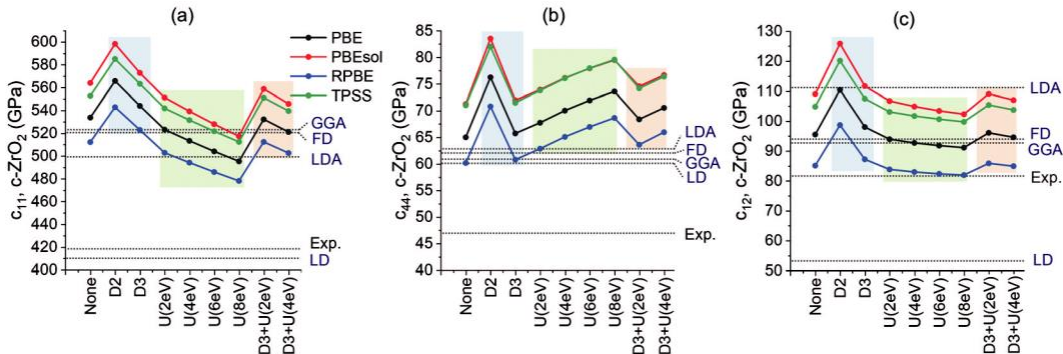


Fig. 3 Computed inequivalent elastic constants (a) c_{11} , (b) c_{44} , and (c) c_{12} (GPa). Previously reported experimental⁵⁷ and theoretical (LDA,⁵² GGA,¹⁴ FD,⁷ and LD⁶⁰) values are also given for comparison. See Table S2 (ESI†).

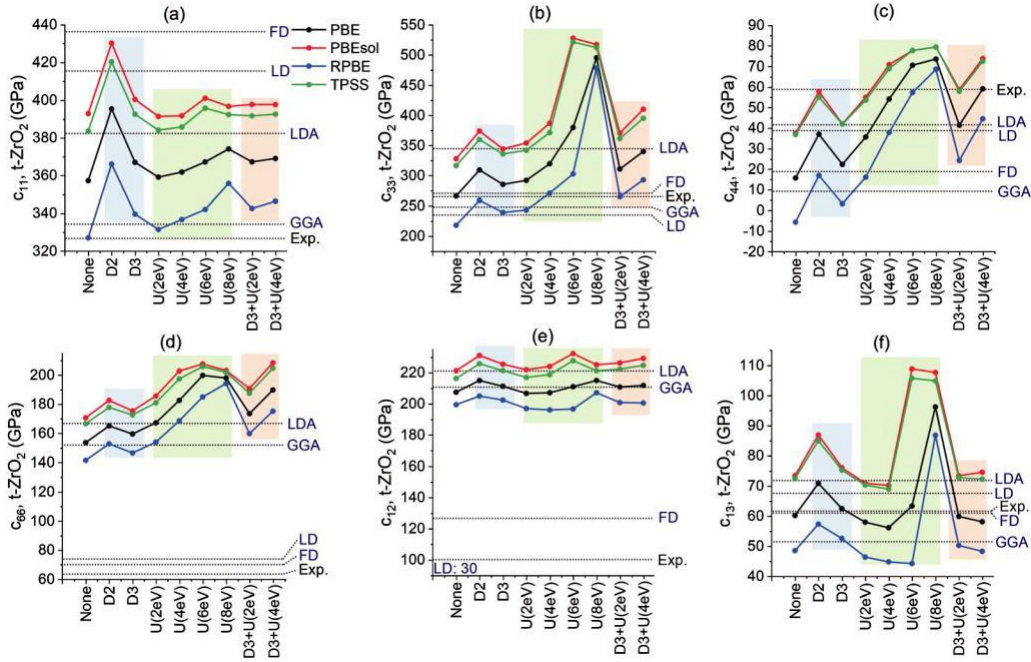


Fig. 4 Computed inequivalent elastic constants (a) c_{11} , (b) c_{33} , (c) c_{44} , (d) c_{66} , (e) c_{12} , and (f) c_{13} (GPa) for t-ZrO₂. Previously reported experimental⁵⁸ and theoretical (LDA,⁵² GGA,¹⁴ FD,⁷ and LD⁶⁰) values are also given for comparison. See Table S3 (ESI†).

values, whereas c_{44} values were underestimated when compared to the experimental values. The elastic constants c_{33} and c_{13} (Fig. 4b and f) were underestimated with standard RPBE and overestimated with standard PBEsol and TPSS, whereas standard PBE gave results that were very close to experimental values. Moreover, the calculated c_{44} (Fig. 4c) using pure RPBE was the only case to give a negative value of the elastic constant.

These variations in trends were also previously observed in other theoretical investigations;^{7,14,52,60} however, for all methodologies tested here, the computed order of magnitude for the elastic constants was $c_{11} > c_{33} > c_{12} > c_{66} > c_{13} > c_{44}$, which is in agreement with the experimental results.⁵⁴ Moreover, two unexpected variations of the computed elastic constants were observed: (i) for c_{11} , c_{44} , and c_{13} , when the D2 correction was included in the calculations, a similar increase in the calculated values as that which was observed for the cubic phase, and (ii) for the calculations using $U = 6$ or 8 eV, particularly for c_{33} and c_{13} , due to the phase transition discussed in the previous subsection.

For m-ZrO₂ (Fig. 5), distinct trends were again observed for the calculated elastic constants. The elastic constants c_{11} and c_{25} (Fig. 5a and k) were underestimated in all methodologies. The elastic constant c_{22} (Fig. 5b) was also underestimated, except when calculated using PBE-D2, PBEsol-D2, PBEsol-D3, TPSS-D2 and TPSS-D3. The computed values for c_{15} , c_{35} , and c_{46} (Fig. 5i, l and m) were all overestimated. Finally, c_{12} and c_{13} (Fig. 5g and h) were also overestimated, using all methodologies except for RPBE and RPBE-D2, respectively. In accordance with previous theoretical results, the elastic components c_{15} and c_{35} (Fig. 5i and l) were obtained as positive values, whereas the experimental values are negative.^{7,9} The only exceptions were

the calculations using RPBE, RPBE+U and PBE+U ($U = 4-8$ eV), which predicted negative values for c_{35} . Similarly, c_{25} (Fig. 5k) was predicted as being negative or close to zero, whilst the experimental value was positive.^{7,9}

We note that unlike our previous calculations for c- and t-ZrO₂, we find that TPSS and PBEsol resulted in less consistent trends for the calculated elastic constants of m-ZrO₂. For c_{33} (Fig. 5c), for instance, unexpected changes are observed in the calculated values when going from $U = 6$ to 8 eV. The inclusion of the D2 dispersion correction also resulted in unexpected trends for some of the calculated elastic constants. As can be seen for c_{11} , c_{33} , c_{13} , and c_{46} (Fig. 5a, c, h, and m), PBE-D2 and RPBE-D2 behaved very differently from PBEsol-D2 and TPSS-D2, the former leading to decrease of the calculated elastic constant when compared to the pure functionals, whereas the latter led to an increase of this property. A higher cutoff energy (750 eV) was also tested and the same trends were observed for these cases (see ESI,† Table S5).

The calculated bulk moduli B_V (Fig. 6) were consistent with all the trends observed above. Inclusion of D2 resulted in large variations of the mechanical properties of the cubic and tetragonal phase, whereas for the monoclinic phase, inclusion of dispersion had distinct effects over PBEsol and TPSS, when compared to PBE and RPBE. In the tetragonal phase, it is possible to observe once again the large variation of B_V for values of $U = 6$ or 8 eV due to the phase transition observed during the optimisation. Finally, the computed B_V for the monoclinic phase shows an unexpected variation observed when using PBEsol and TPSS. For the cubic and tetragonal phases, RPBE was again the methodology that afforded the closest match to experimental values, followed by PBE, TPSS,

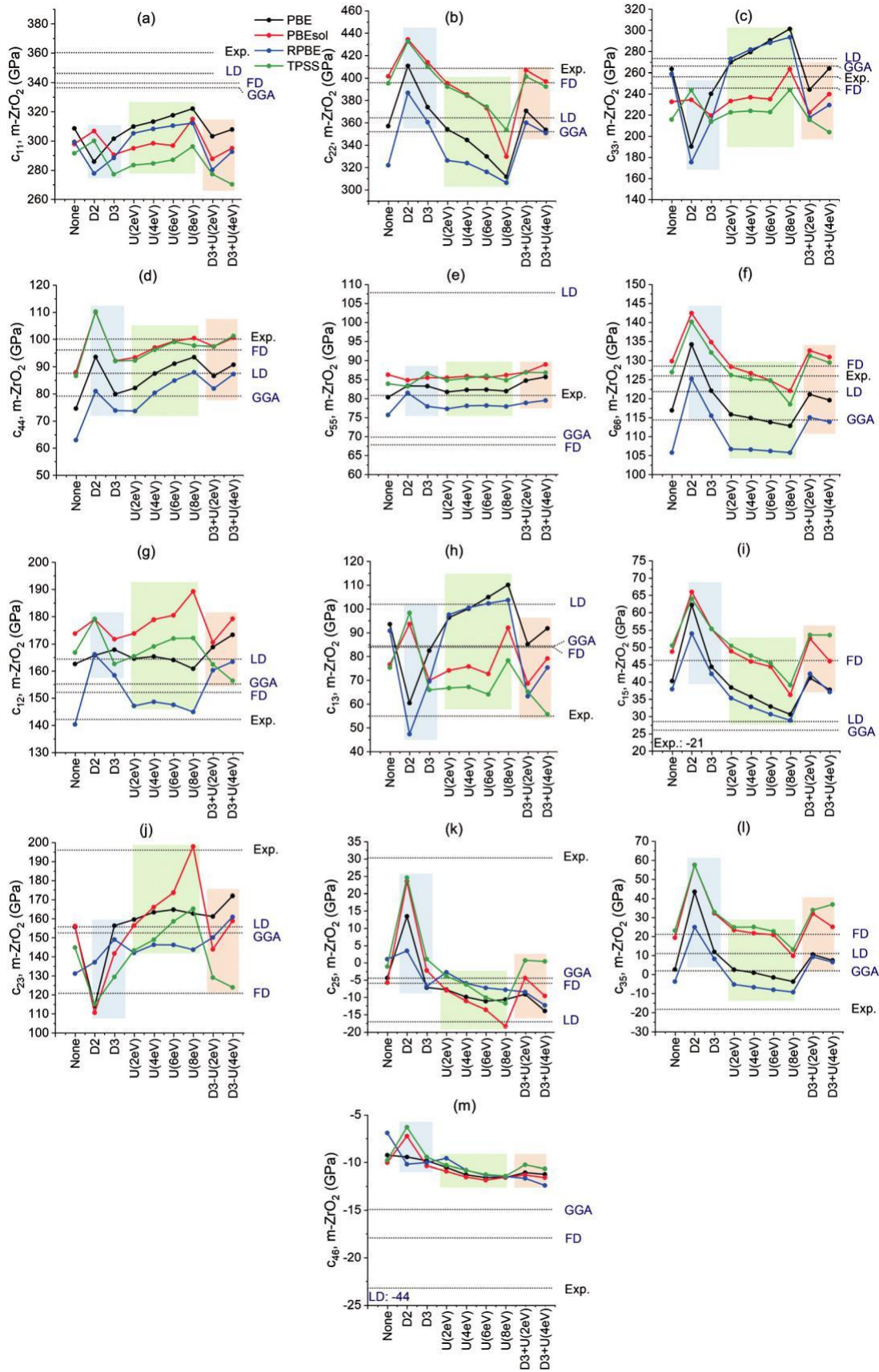


Fig. 5 Computed inequivalent elastic constants (a) c_{11} , (b) c_{22} , (c) c_{33} , (d) c_{44} , (e) c_{55} , (f) c_{66} , (g) c_{12} , (h) c_{13} , (i) c_{15} , (j) c_{23} , (k) c_{25} , (l) c_{35} , and (m) c_{46} (GPa) for m-ZrO₂. Previously reported experimental⁵⁹ and theoretical (GGA,¹⁴ FD,⁷ and LD⁶⁰) values are also given for comparison. See Table S4 (ESI†).

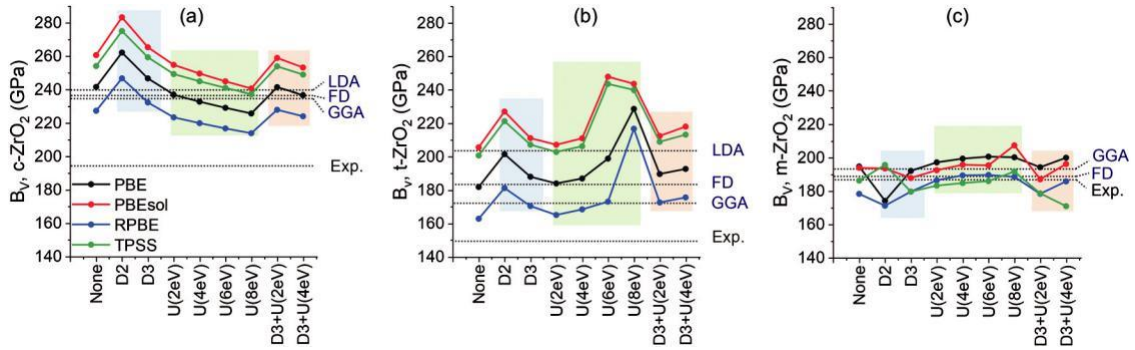


Fig. 6 Computed bulk modulus B_V (GPa) for (a) c-, (b) t-, and (c) m-ZrO₂. Previously reported experimental^{57–59} and theoretical (LDA,⁵² GGA,¹⁴ FD,⁷ and LD⁶⁰) values are also given for comparison. See Tables S2–S4 (ESI†).

and PBEsol, although TPSS and PBEsol gave in general very similar results. For the monoclinic phase, all methodologies gave values similarly close to the experimental results.

The shear modulus (G), Young's modulus (E), and Poisson ratio (ν) derived from the calculated elastic constants are presented in the ESI† (Tables S2–S4).

c. Dielectric properties

The calculated dielectric tensor ϵ , as well as the computed electronic and ionic contributions (ϵ^N and ϵ^{ion}) for the three zirconia phases are shown in Fig. 7–9. Previously reported experimental^{9,63,64} and theoretical values are given for comparison. The previously reported theoretical values were calculated using LDA and GGA (PBE) functionals by Density Functional Perturbation Theory (DFPT/ LDA and DFPT/PBE, respectively)^{9,61,62} and by Finite Difference (LD/LDA)¹⁸ method. For these cases, the data for TPSS are not shown since the linear response method using Meta-GGA functionals are not supported by the software used for these calculations.

For c-ZrO₂, only the matrix tensors of the electronic and ionic contributions ϵ^N_{11} and $\epsilon^{\text{ion}}_{11}$ are shown in Fig. 7, as $\epsilon^N_{11} = \epsilon^N_{22} = \epsilon^N_{33} = \epsilon^N$ and $\epsilon^{\text{ion}}_{11} = \epsilon^{\text{ion}}_{22} = \epsilon^{\text{ion}}_{33} = \epsilon^{\text{ion}}$. The three functionals resulted in similar values of ϵ^N_{ij} , with only small variations observed when dispersion was included in the calculation. The inclusion of the Hubbard correction, on the other hand, resulted in a significant reduction of the calculated values,

from 5.8–5.9 to 4.5–4.7. For $\epsilon^{\text{ion}}_{ij}$ a slight variation is observed between the three functionals, with RPBE giving the higher values, followed by PBE and PBEsol. These differences between functionals were observed to decrease with inclusion of Hubbard corrections, whilst the computed ϵ_{ij} value also dropped significantly. Overall, the calculated total dielectric constant ϵ was overestimated when using the standard functionals and inclusion of dispersion and Hubbard correction led to a decrease of the calculated ϵ . For all functionals, calculations using $U = 2$ or 4 eV with or without D3 gave the closest results to the experimental values.

The calculated electronic contributions to the dielectric tensor of t-ZrO₂ (Fig. 8) were only slightly anisotropic, whereas the ionic contributions show much larger differences between the computed tensor components. As before, the three functionals behaved similarly, except for the ϵ^{ion} calculated using RPBE, RPBE-D2 and RPBE-D3, which afforded unexpectedly high values. Nevertheless, this deviation was satisfactorily corrected when Hubbard corrections were included in the calculation. In all cases, values of U higher than 4 eV led to underestimation of the dielectric constant when compared to the experimental values.

Despite the phase transition observed for the tetragonal phase at high values of U , the variation of the contributions to the dielectric constant were smooth, except for $\epsilon^{\text{ion}}_{33}$. However, the total ionic contributions, as well as the total dielectric

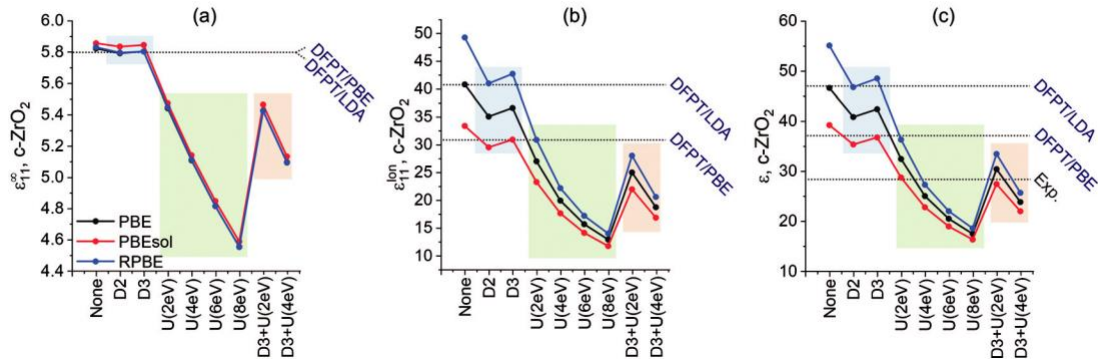


Fig. 7 Electronic (a, ϵ^N_{11}) and ionic (b, $\epsilon^{\text{ion}}_{11}$) contributions to the dielectric tensor, and total dielectric constant (c, ϵ) of c-ZrO₂. Previously reported experimental^{9,63,64} and theoretical (DFPT/LDA and DFPT/PBE)^{9,61,62} values are presented for comparison. See Table S6 (ESI†).

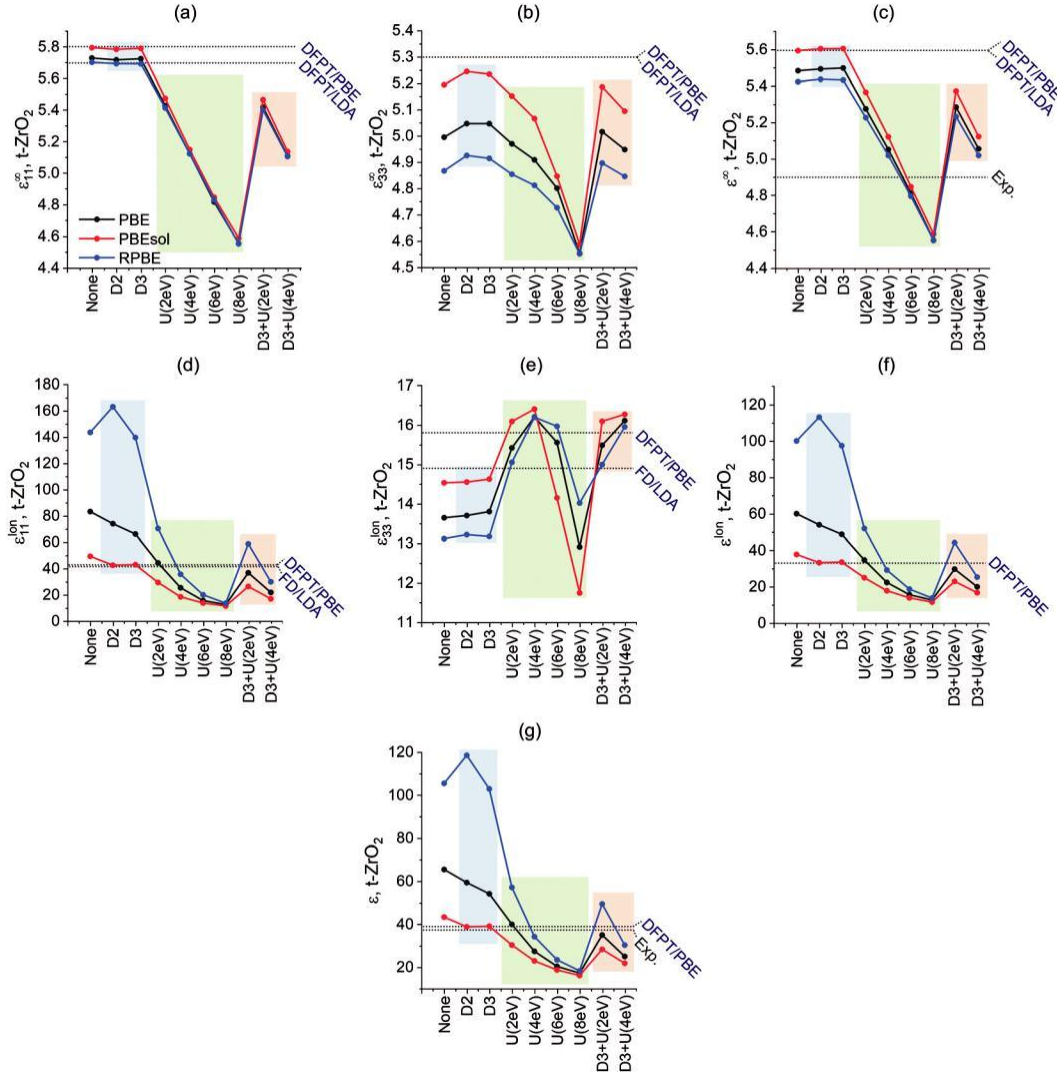


Fig. 8 Electronic (a and b, ϵ^N_{11} and ϵ^N_{33}) and ionic (d and e, $\epsilon^{\text{ion}}_{11}$ and $\epsilon^{\text{ion}}_{33}$) contributions to the dielectric tensor, total electronic (c, ϵ^N) and ionic contributions (f, ϵ^{ion}), and total dielectric constant (g, ϵ) of t-ZrO₂. Previously reported experimental^{9,63,64} theoretical (DFPT/LDA, DFPT/PBE, and FD/LDA)^{9,18,61,62} are presented for comparison. See Table S7 (ESI†).

constant still presented smooth variations throughout the methodologies investigated.

Finally, all calculated contributions to the dielectric constant of m-ZrO₂ (Fig. 9) presented similar trends for the distinct functionals and resulted in only slight variations amongst different methodologies. Calculated values of ϵ^N were very close to experiment when U (U = 4 eV) and D3+U (U = 4 eV) were used, whereas higher values of U once again led to underestimated values. However, the calculated ϵ using U (U = 4 eV) and D3+U (U = 4 eV) were slightly smaller than the experimental values.

In summary, inclusion of dispersion corrections resulted in only small changes in the calculated dielectric constants for all the cases investigated here, as also observed in the previous subsections. In all cases, however, inclusion of Hubbard correction (U = 4 eV or larger) resulted in a large reduction of the calculated dielectric constants, which eventually led to the underestimation of the calculated values when compared to the experimental ones. In general, all functionals behaved

much alike, except for when standard RPBE and RPBE-D were used to calculate the dielectric constants of t-ZrO₂. In this case, the calculated dielectric constants were largely overestimated and inclusion of the Hubbard correction appears to be necessary for better prediction of these property. In general, RPBE+U and RPBE-D3+U had the best results amongst the functionals tested when U = 4 eV was used. When the standard functionals, DFT-D, DFT+U(2 eV), or DFT-D3+U(2 eV) were employed, PBEsol gave the closest results to the experimental values, followed by PBE and RPBE.

Refractive indices (n) derived from the calculated dielectric constants are presented in the ESI† (Tables S6–S8).

d. Electronic properties

The energy band structure and density of states of the three polymorphs of zirconia were obtained using all DFT methods employed in this survey. However only representative examples are shown here, i.e., those using the standard functionals, as

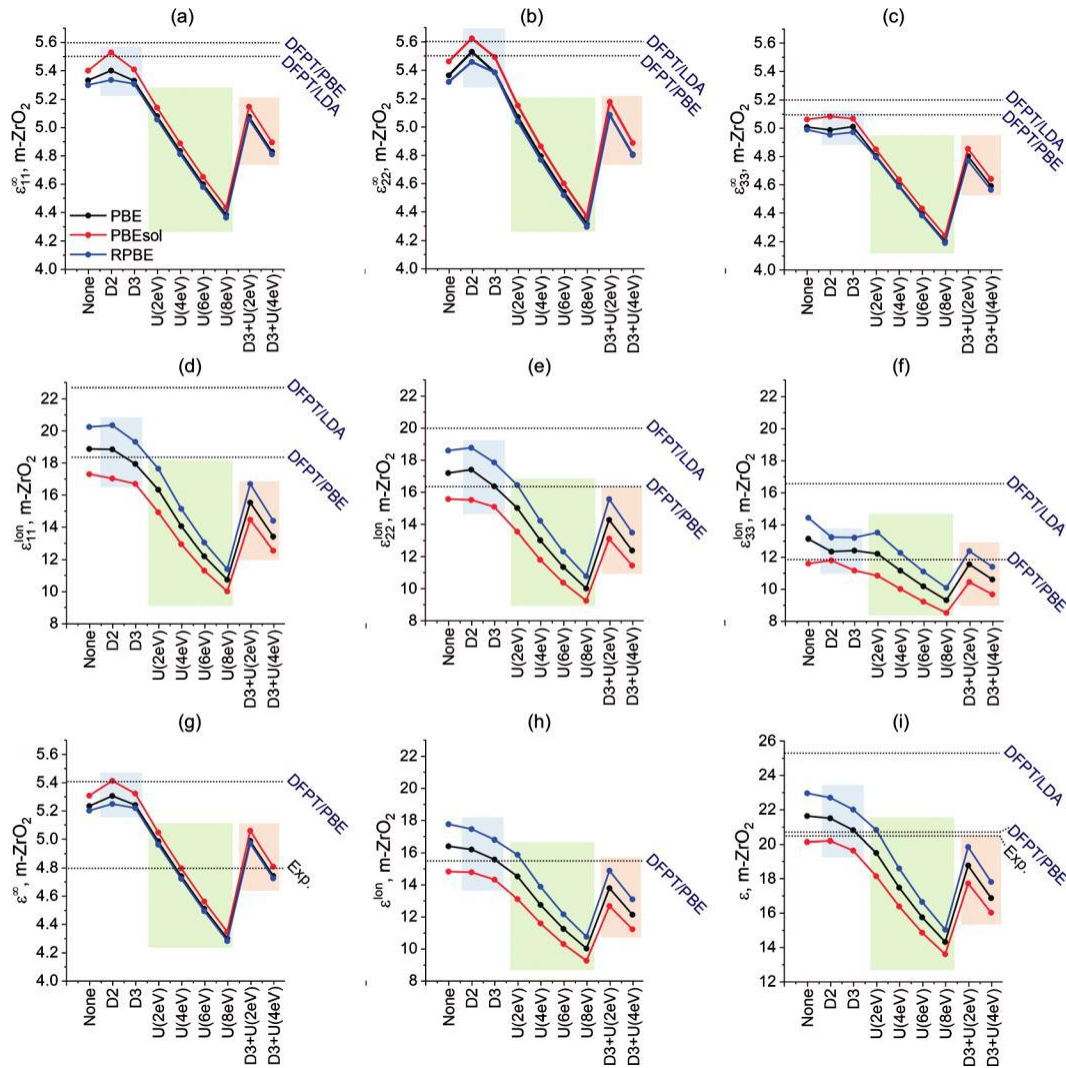


Fig. 9 Electronic (a–c, $\epsilon^{N_{11}}$, $\epsilon^{N_{22}}$, and $\epsilon^{N_{33}}$) and ionic (d–f, $\epsilon^{\text{ion}}_{11}$, $\epsilon^{\text{ion}}_{22}$, and $\epsilon^{\text{ion}}_{33}$) contributions to the dielectric tensor, total electronic (g, ϵ^N) and ionic contributions (h, ϵ^{ion}), and total dielectric constant (i, ϵ) of m-ZrO₂. Previously reported experimental^{9,63,64} and theoretical (DFPT/LDA and DFPT/PBE)^{9,61,62} values are presented for comparison. See Table S8 (ESI†).

Table 4 Calculated band gap for c-ZrO₂. Previously reported experimental⁶² and theoretical (PBE)¹² values are presented for comparison

| E_g | PBE | PBEsol | RPBE | TPSS |
|----------------------------|---------------|---------------|---------------|----------------|
| None | 3.309 (G - G) | 3.317 (G - G) | 3.298 (G - G) | — ^a |
| D2 | 3.369 (G - G) | 3.370 (G - G) | 3.361 (G - G) | — ^a |
| D3 | 3.345 (G - G) | 3.344 (G - G) | 3.347 (G - G) | — ^a |
| U(2 eV) | 3.588 (G - G) | 3.596 (G - G) | 3.579 (G - G) | — ^a |
| U(4 eV) | 3.886 (G - G) | 3.893 (G - G) | 3.878 (G - G) | 0.089 (G - G) |
| U(6 eV) | 4.153 (G - G) | 4.134 (G - G) | 4.185 (G - G) | 0.496 (G - G) |
| U(8 eV) | 4.310 (G - G) | 4.280 (G - G) | 4.350 (G - G) | 0.833 (G - G) |
| D3+U(2 eV) | 3.624 (G - G) | 3.623 (G - G) | 3.627 (G - G) | — ^a |
| D3+U(4 eV) | 3.922 (G - G) | 3.920 (G - G) | 3.926 (G - G) | 0.091 (G - G) |
| Experimental ⁶² | 6.10 | | | |
| PBE ¹² | 3.319 (X - G) | | | |

^a Metallic-like band structure was obtained.

well as the cases in which dispersion (D3) and $U = 4$ eV were included. All calculated band gaps are presented in Tables 4–6, while Fig. 10 shows the calculated band structure and density of states of c-, t-, and m-ZrO₂ obtained using standard PBE.

Fig. 11 and 12 show the band structure and density of states of c-ZrO₂ calculated when additional corrections (D3 and/or $U = 4$ eV) were used with PBE (Fig. 11) and when the four standard functionals were applied (Fig. 12). As the variations observed

Table 5 Calculated band gap for t-ZrO₂. Previously reported experimental⁶² and theoretical (PBE)¹² values are presented for comparison

| | PBE | PBEsol | RPBE | TPSS |
|----------------------------|---------------------------------|---------------------------------|----------------|----------------|
| None | 4.043 (Z-G) | 4.005 (Z - G) and 4.012 (A - G) | 4.071 (Z - G) | 0.672 (Z-G) |
| D2 | 4.085 (Z-G) | 4.013 (A-G) | 4.111 (Z - G) | 0.848 (Z-G) |
| D3 | 4.057 (Z-G) | 4.000 (A-G) | 4.102 (Z - G) | 0.827 (Z-G) |
| U(2 eV) | 4.189 (Z - G) and 4.192 (A - G) | 4.073 (A-G) | 4.206 (Z - G) | 0.832 (A-G) |
| U(4 eV) | 4.279 (A-G) | 4.065 (M-G) | 4.364 (A - G) | 0.962 (M-G) |
| U(6 eV) | — ^a | — ^a | — ^a | — ^a |
| U(8 eV) | — ^a | — ^a | — ^a | — ^a |
| D3+U(2 eV) | 4.176 (A-G) | 4.063 (A-G) | 4.242 (Z - G) | 0.823 (A-G) |
| D3+U(4 eV) | 4.259 (M - G) and 4.265 (A - G) | 4.009 (M-G) | 4.367 (A - G) | 0.855 (M-G) |
| Experimental ⁶² | | 5.78 | | |
| PBE ¹² | | 4.076 (Z - G) | | |

^a Phase transition observed (t-ZrO₂ - c-ZrO₂).

Table 6 Calculated band gap for m-ZrO₂. Previously reported experimental⁶² and theoretical (PBE)¹² values are presented for comparison

| | PBE | PBEsol | RPBE | TPSS |
|----------------------------|---------------|---------------------------------|---------------|-------------|
| None | 3.631 (G - Y) | 3.574 (G-Y) | 3.702 (G - Y) | 1.167 (G-Y) |
| D2 | 3.758 (G - Y) | 4.067 (G - Y) and 4.076 (G - G) | 3.668 (G - Y) | 1.045 (G-G) |
| D3 | 3.616 (G - Y) | 3.598 (G-Y) | 3.680 (G - Y) | 1.174 (G-Y) |
| U(2 eV) | 3.762 (G - Y) | 3.726 (G-Y) | 3.806 (G - Y) | 1.357 (G-Y) |
| U(4 eV) | 3.934 (G - Y) | 3.897 (G-Y) | 3.971 (G - Y) | 1.646 (G-Y) |
| U(6 eV) | 4.130 (G - Y) | 4.085 (G-Y) | 4.166 (G - Y) | 1.790 (G-Y) |
| U(8 eV) | 4.343 (G - Y) | 4.294 (G-Y) | 4.380 (G - Y) | 2.088 (G-Y) |
| D3+U(2 eV) | 3.761 (G - Y) | 3.758 (G-Y) | 3.822 (G - Y) | 1.349 (G-Y) |
| D3+U(4 eV) | 3.936 (G - Y) | 3.929 (G-Y) | 4.002 (G - Y) | 1.549 (G-Y) |
| Experimental ⁶² | | 5.83 | | |
| PBE ¹² | | 3.698 (G - B) | | |

for the three polymorphs of zirconia (c-, t-, and m-ZrO₂) were very similar, only the band structures of c-ZrO₂ are presented in the main text. All comparisons for t- and m-ZrO₂ can be found in ESI† (Fig. S4–S10).

As reported by previous theoretical investigation,²³ it is possible to observe in Fig. 10 that in all cases the upper valence band is mainly formed by oxygen 2p states with minor presence of zirconium 4d states. The bottom of the conduction band, on the other hand, is mainly formed by 4d states. Interestingly, for c- and t-ZrO₂ the bottom of the conduction band is separated from the rest of the that band, although the same is not calculated for m-ZrO₂.²² The calculated band structure using standard PBE shows that c-ZrO₂ presents a direct G - G band gap of about 3.3 eV, whereas t- and m-ZrO₂ presents indirect band gaps of about 4.0 eV (Z - G) and 3.6 eV (G - Y), respectively. As expected, all calculated band gaps were under-estimated when compared to the experimental values (E_g = 6.10 eV for c-ZrO₂, 5.78 eV for t-ZrO₂, and 5.83 eV for m-ZrO₂, Tables 4–6),⁶² which is a well-known effect observed in DFT calculations, especially when using LDA, GGA, and Meta-GGA functionals.²⁸ In accordance with previous investigations, the Width of the Upper Valence Band (WUVB) increased from c-ZrO₂ to t-ZrO₂ and from t-ZrO₂ to m-ZrO₂.^{12,22} The calculated WUVB using standard PBE were 5.83 eV, 5.00 eV, and 4.90 eV for c-, t-, and m-ZrO₂, respectively.

Inclusion of the D3 dispersion correction in the calculations using PBE (Fig. 11) only led to small variations of the calculated band structures for c-ZrO₂. On the other hand, when the Hubbard correction was used, a systematic increase in the calculated band

gaps is observed, from 3.309 eV to 3.886 eV for PBE and PBE+U(4 eV), and from 3.345 eV to 3.922 eV for PBE-D3 and PBE-D3+U(4 eV). Previously studies have reported an indirect

X - G transition for c-ZrO₂ as that presenting the lowest band gap,^{8,35,65} however in the present work the same indirect X - G transition presented a band gap value of 3.913 eV, 0.6 eV larger than the computed direct G - G transition. No major differences between the direct and indirect band gaps were observed for any of the methodologies tested (Table 4).

The addition of both dispersion and Hubbard correction resulted in distinct trends for the calculated Width of the Upper Valence Band (WUVB) obtained for c-ZrO₂. When PBE+U(4 eV) was used, a reduction of 0.18 eV was observed in the WUVB when compared to standard PBE. On the other hand, the calculated WUVB obtained using PBE-D3 or PBE-D3+U(4 eV) were slightly larger than the corresponding calculation without D3 correction, resulting in an increase of 0.07 and 0.06 eV, respectively.

Band gaps calculated using standard PBEsol and RPBE (Fig. 12) did not present significant changes from that calculated using standard PBE. The essential features remain the same and a similar comparison as that shown in Fig. 11 can be found in the ESI† for RPBE (Fig. S4). Similar behaviour has been observed before for GGA and hybrid functionals.^{8,40} TPSS, on the other hand, resulted in even lower band gaps, in some cases yielding a metallic-like band structure with the conduction and valence bands overlapped. When U = 4 eV or higher was used, the overlap disappeared but the resulting band gap was still much smaller than those calculated with the GGA functionals. The calculated WUVB also only presented small

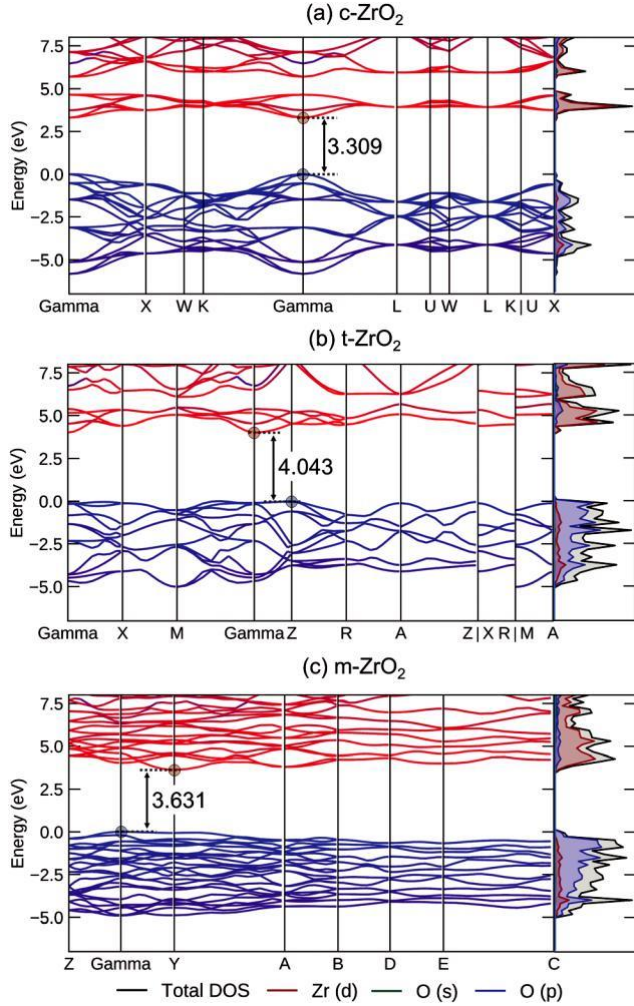


Fig. 10 Band structures (left) and density of states (right) of (a) c-, (b) t-, and (c) m-ZrO₂ calculated using standard PBE. The top of the valence band is taken a zero of energy.

variations between functionals, with computed values of 5.83, 6.10, and 5.66 eV for PBE, PBEsol, and RPBE, respectively.

It is well-known that a better description of band structures by DFT methods can be achieved using hybrid functional, as has been demonstrated for HSE03, HSE06, PBE0, B3LYP, amongst others.^{8,39–41} These functionals can afford band gap values much closer to experiment than those calculated using GGA or Meta-GGA methods. Nevertheless, these functionals would be prohibitively expensive for the calculation of the range of properties reported in this paper, which as we show can be modelled by the less expensive approaches which we have employed. Interestingly, our work demonstrates that a similar approximation of the experimental band structure of ZrO₂ polymorphs can be achieved with the much cheaper Hubbard U corrected GGA methodologies.

The trends observed for t- and m-ZrO₂ are similar to those discussed above for c-ZrO₂; however, we note that the position of the indirect transition observed for t-ZrO₂ was highly dependent on the methodology used, as shown in Table 5. For instance, it was observed for t-ZrO₂ that inclusion of U led the indirect

Z - G transition to be altered into an indirect A - G transition, followed by an indirect M - G transition when higher values of U were used. In three cases (PBEsol, PBE+U(2 eV), and PBE-D3+U(2 eV)) two nearly degenerate indirect transitions were observed, with a difference in band gap smaller than 0.01 eV. For m-ZrO₂, besides the indirect G - Y mentioned before (Table 6), PBEsol-D2 also gave a close to degenerate G - G transition, with band gap values larger than that of G - Y transition by less than 0.01 eV.

Overall, the calculated band gaps agreed well with previous theoretical investigation, although they were underestimated when compared to experimental values, as expected for calculations using GGA or meta-GGA functionals.²⁸ Regarding the different functionals tested here, the band structures obtained were mostly unchanged, except for TPSS which afforded in most cases much smaller band gaps or even metallic-like band structures. As also found in the previous subsections, dispersion had only small effects on the calculated band gaps, whereas inclusion of Hubbard correction led to a systematic increase of the band gap up to 4.4 eV when U = 8 eV. However, as highlighted in the previous subsections, values of U larger than 4 eV should be avoided in these calculations due to the deterioration observed in the description of structural parameter, relative energies and dielectric constants. As a result, the highest band gaps (and therefore most consistent with the experimental values) which it is possible to obtain while still conserving a good compromise with other bulk properties of ZrO₂ should be those calculated using U = 4 eV (for RPBE) or U = 2 eV (for PBE and PBEsol).

e. Phonon dispersion curves

The phonon dispersion curves for c-, t-, and m-ZrO₂ calculated using PBE, PBE+U(4 eV), and PBEsol are shown in Fig. 13. Additional comparisons using RPBE or dispersion correction can be found in the ESI† (Fig. S11–S13). We note that Born effective charges and longitudinal optical/transverse optical (LO/TO) splitting at gamma point were not included in these calculations. Nevertheless, the comparison of DFT methodologies and their systematic variation for the description of the phonon dispersion curves as discussed here should not be significantly altered by such corrections. Additionally, results of phonon dispersion curves for ZrO₂ including the longitudinal optical/ transverse optical (LO/TO) splitting have been reported before.^{17,61}

Dispersion correction D3 had only a small effects on the calculated dispersion curves, leading to slight increase of the calculated frequencies, but without significant modification of the dispersion curves. The inclusion of the Hubbard correction had distinct effects over the three zirconia phases, in general leading to the disappearance of unphysical imaginary frequencies observed in the structures, as will be detailed below.

The phonon dispersion curves calculated for c-ZrO₂ presented imaginary frequencies at the X, W, K, and U points when standard PBE was used (Fig. 13a). When using PBEsol, imaginary frequencies were observed at the points X, K, and U (Fig. 13b), in agreement with previous calculations using PBEsol/DFPT.⁶⁶ Finally, only one negative frequency at the X point was observed

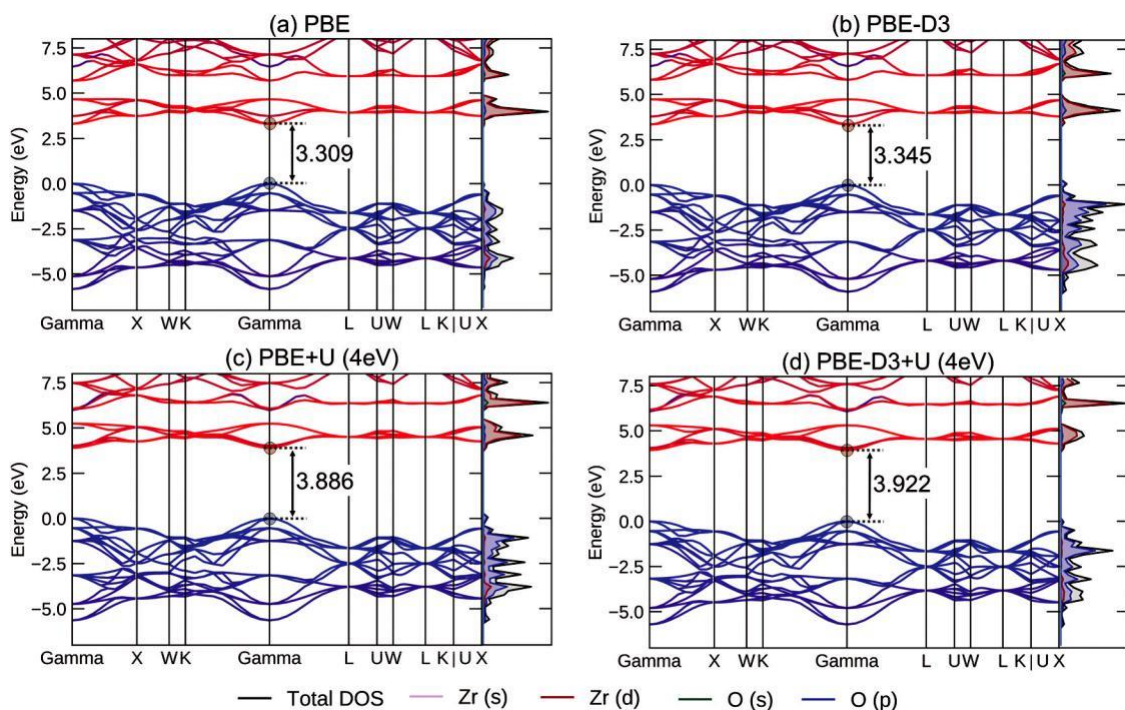


Fig. 11 Band structures (left) and density of states (right) of c-ZrO₂ calculated using standard (a) PBE, (b) PBE-D3, (c) PBE+U (U = 4 eV), and (d) PBE-D3+U (U = 4 eV). The top of the valence band is taken as zero of energy.

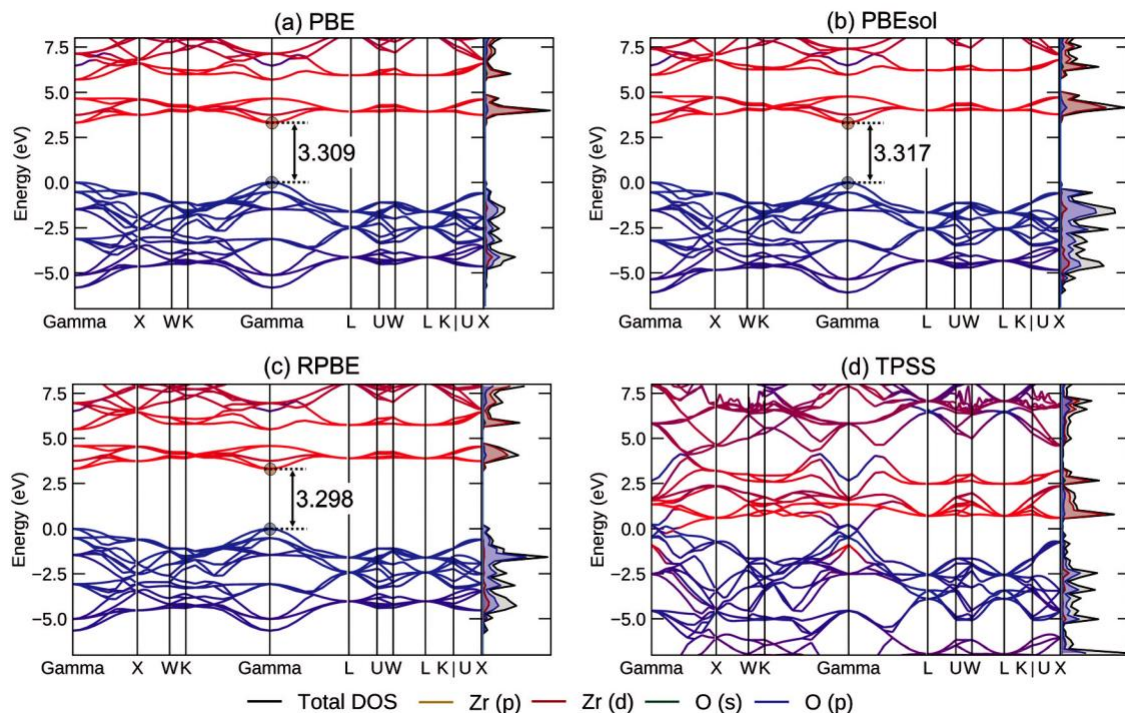


Fig. 12 Band structures (left) and density of states (right) of c-ZrO₂ calculated using standard (a) PBE, (b) PBEsol, (c) RPBE, and (d) TPSS. The top of the valence band is taken as zero of energy.

for c-ZrO₂ when PBE+U(4 eV) was used (Fig. 13a). Such imaginary frequency at the X point (X_2^-) in c-ZrO₂ have been reported before as corresponding to the eigenmode responsible for the oxygen displacement in the structure leading to t-ZrO₂.^{16,17,67}

Such an observation is expected for this polymorph, since c-ZrO₂ is unstable at low temperatures and it is promptly converted into t-ZrO₂ or m-ZrO₂. The functionals PBE and RPBE behaved much alike in this case, as can be seen in Fig. S11 (ESI†).

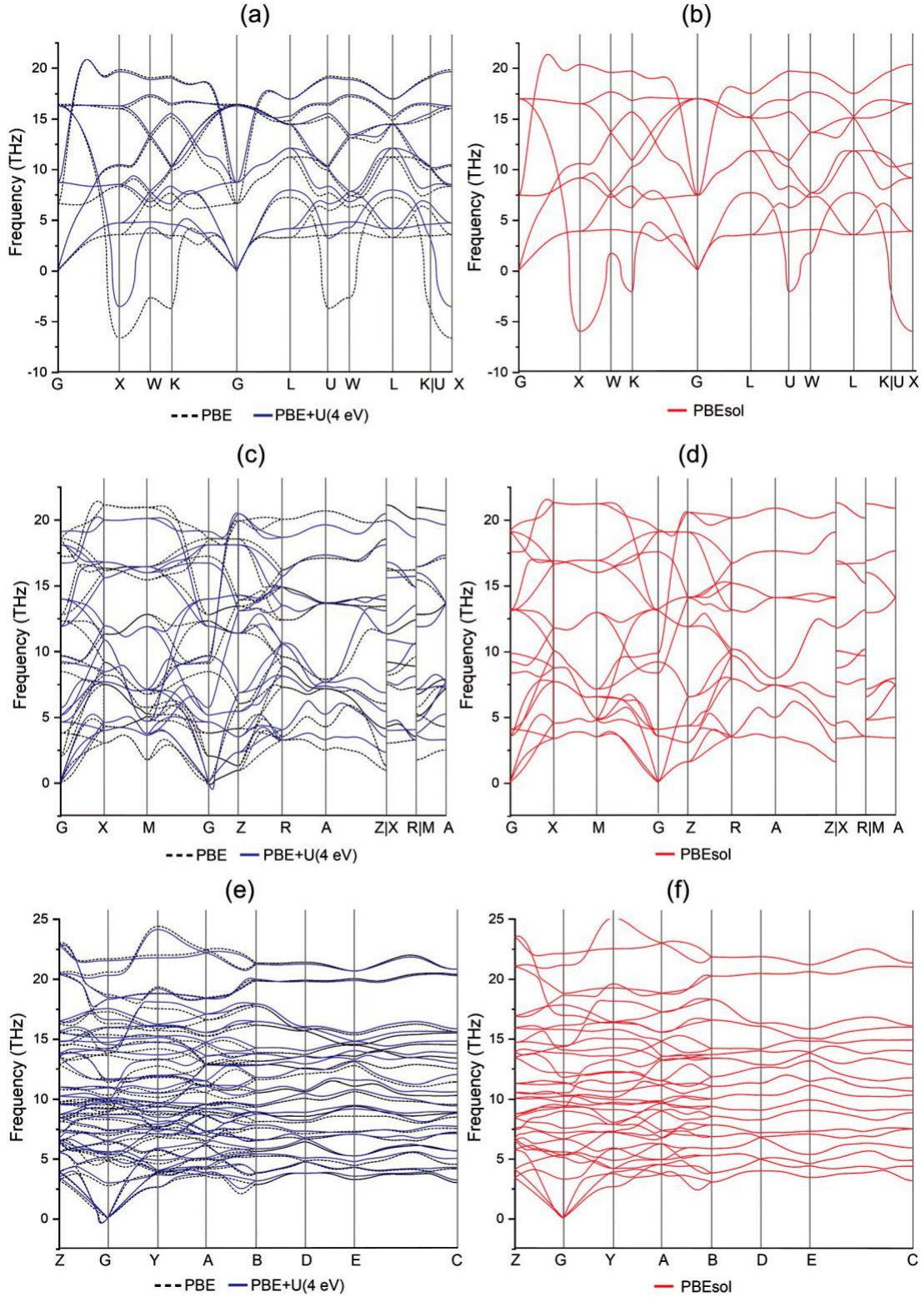


Fig. 13 Phonon dispersion curves of c- (a and b), t- (c and d), and m-ZrO₂ (e and f) calculated using PBE, PBE+U(4 eV), and PBEsol.

For t-ZrO₂, both PBE and PBE+U(4 eV) yielded phonon dispersion curves with only positive frequencies, except for one small imaginary frequency (0.7i THz) at the vicinity of the gamma point, which may be associated with the limitation of the supercell size

(Fig. 13c).¹⁶ For PBEsol, however, such an imaginary frequency was not observed (Fig. 13d). We note that the Hubbard correction had a larger effect on the higher frequencies (410 THz) than for c-ZrO₂, probably due to the structural distortion caused by

the addition of the U correction to the calculation, as discussed in the previous subsections. Standard RPBE failed to describe the phonon dispersion curves of t-ZrO₂ as imaginary frequencies are observed at the points M and Z, as well as around the gamma point (Fig. S12, ESI†). Nevertheless, the results for t-ZrO₂ (RPBE) are fully corrected by addition of the Hubbard correction to the calculations, with RPBE+U(4 eV) yielding a dispersion curve much like those obtained using PBE and PBE+U(4 eV).

As was observed for t-ZrO₂, the phonon dispersion curves of m-ZrO₂ calculated using PBE and PBE+U(4 eV) yielded one small imaginary frequency (0.7i THz) at the vicinity of the gamma point, whereas PBEsol gave only positive frequency values. Once again, very similar behavior was observed for calculation using RPBE and RPBE+U(4 eV), as shown in Fig. S13 (ESI†).

In general, dispersion correction D3 had only a small effect on the calculated phonon dispersion curves, whereas the Hubbard correction resulted in much larger modifications to the calculated dispersion curves of PBE and RPBE. For all phases PBE+U and RPBE+U behaved similarly, affording results close to previously reported calculations and in agreement with the expected stability and number of imaginary frequencies in each phase. The only exception was a small imaginary frequency (0.7i THz) observed at the vicinity of the gamma points of t- and m-ZrO₂. Standard PBEsol, on the other hand did not result in any imaginary for t- and m-ZrO₂. For the calculation of the phonon dispersion curves using PBE and RPBE, the inclusion of the Hubbard correction was necessary to correct unexpected imaginary frequencies in c- and t-ZrO₂. When standard PBEsol was used, on the other hand, the calculated dispersion curves were similar to those obtained using PBE+U and RPBE+U.

Only limited experimental lattice dynamical data are available for zirconia and it would be of considerable interest to obtain experimental data to compare with our predictions.⁴²

Summary and conclusions

Four distinct DFT functionals (PBE, PBEsol, RPBE, and TPSS) were investigated for the description of the bulk properties of m-, t-, and c-ZrO₂. The inclusion of dispersion (Grimme's D2 and D3 approach) and on-site Coulomb repulsion corrections (Hubbard term, U ranging from 2 to 8 eV) were also considered in order to thoroughly compare the simultaneous performance of such DFT approaches in the description of structural, elastic, mechanical, and dielectric properties, as well as relative phase stability, electronic structure, and phonon dispersion curves.

In general, the use of the Hubbard correction was demonstrated to be necessary for an improvement of all bulk properties investigated here. When values of U = 2 or 4 eV were used, despite a slight deterioration in the description of structure parameters, deviation of elastic constants, dielectric constants, and band gaps from the experimental values was significantly reduced. Calculated phonon dispersion curves were also significantly improved when U was used, affording results close to previously reported calculations and in agreement with the

expected stability and number of imaginary frequencies in each phase. Nevertheless, it has been clearly demonstrated that care needs to be taken in the choice of the U parameter, as U values larger than 2 eV (4 eV for RPBE) can lead to t-ZrO₂ - c-ZrO₂ phase transition, inversion of relative stability between c- and m-ZrO₂, and give largely underestimated dielectric constants.

Considering the set of functionals investigated here, when the standard functional is used without additional corrections, PBEsol and TPSS yielded the best results on structural properties of ZrO₂, whereas PBE and RPBE performed better than these functionals when dispersion corrections (especially, D3) were included in the calculation of the structural parameters. Interestingly, despite the lower performance of RPBE in the description of structural properties of zirconia, this functional gave the best prediction of elastic and mechanical properties of the three polymorphs investigated, regardless of whether additional corrections were used or not. Standard PBEsol was the best functional for describing the dielectric constants and phonon dispersion curves of ZrO₂. Additionally, PBEsol-D and PBEsol+U(2 eV) also resulted in the best estimate of the dielectric constants when compared to PBE and RPBE. When U = 4 eV (in combination with D3 or not) was used, however, RPBE was the functional to give the closest dielectric constants to the experimental values. Standard PBE and RPBE were unable to reproduce faithfully the phonon dispersion curves of ZrO₂. However, inclusion of U resulted in a significant correction of this property, yielding phonon dispersion curves of ZrO₂ in agreement with previous reports. Calculated band gaps and band structures were mostly unchanged when different functionals were used. However, we note that RPBE was the only functional to conserve the distinct structures and stabilities of c-, t-, and m-ZrO₂ when U = 4 eV was included in the calculation. As a result, RPBE was the functional able to afford the highest correction of the calculated band structures by inclusion of Hubbard corrections, affording the best estimate of the band gaps of ZrO₂.

Overall, we find that DFT techniques can reproduce a wide range of bulk properties of ZrO₂ but that the most appropriate functional may depend on the property under study. Furthermore, our results demonstrate that the appropriate choice of methodologies is crucial for computing accurate properties of this material and that the incorrect choice will result in unreliable or unphysical results. Our survey demonstrates that it is possible to provide a consistent theoretical description of the properties of the polymorphs of zirconia and should provide a firm foundation for future investigations of this important and intensively studied material.

Conflicts of interest

There are no conflicts to declare.

Acknowledgements

This work used the computing facilities provided by ARCCA at Cardiff University (HPC Wales), GW4 Isambard "Phase 2" – ARM

XC50 at Bristol University, the Cirrus UK National Tier-2 HPC Service at EPCC (<http://www.cirrus.ac.uk>) funded by the University of Edinburgh and EPSRC (EP/P020267/1), and the ARCHER facility through our membership of the UK's HEC Materials Chemistry Consortium, which is funded by EPSRC (EP/L000202). We are also grateful for access to the THOMAS computational facility managed by the UK Materials and Molecular Modelling Hub, which is partially funded by EPSRC (EP/P020194). The UK Catalysis Hub is kindly thanked for resources and support provided funded by EPSRC (Grants EP/I038748/1, EP/I019693/1, EP/K014706/1, EP/K014668/1, EP/K014854/1, EP/K014714/1, and EP/M013219/1).

Notes and references

- R. G. Luthardt, M. Holzhueter, O. Sandkuhl, V. Herold, J. D. Schnapp, E. Kuhlisch and M. Walter, *J. Dent. Res.*, 2002, 81, 487.
- L. Jin, Q. Yu, A. Rauf and C. Zhou, *Solid State Sci.*, 2012, 14, 106.
- F. H. Garzon, R. Mukundan, R. Lujan and E. L. Brosha, *Solid State Ionics*, 2004, 175, 487.
- F. Fleischhauer, R. Bermejo, R. Danzer, A. Mai, T. Graule and J. Kuebler, *J. Power Sources*, 2015, 273, 237.
- S. H. Messaddeq, S. H. Pulcinelli, C. V. Santilli, A. C. Guastaldi and Y. Messaddeq, *J. Non-Cryst. Solids*, 1999, 247, 164.
- R. C. Garvie, R. H. Hannink and R. T. Pascoe, *Nature*, 1975, 258, 703.
- Y. Zhang, H.-X. Chen, L. Duan, J.-B. Fan, L. Ni and V. Ji, *J. Alloys Compd.*, 2018, 749, 283.
- Y.-L. Yang, X.-L. Fan, C. Liu and R.-X. Ran, *Phys. B*, 2017, 434, 7.
- Y. Zhang, H.-X. Chen, L. Duan, J.-B. Fan, L. Nia and V. Ji, *Solid State Sci.*, 2018, 81, 58.
- D. L. Wood and K. Nassau, *Appl. Opt.*, 1982, 21, 2978.
- G. P. Cousland, X. Y. Cui, A. E. Smith, A. P. J. Stampfl and C. M. Stampfl, *J. Phys. Chem. Solids*, 2018, 122, 51.
- Z. Liang, W. Wang, M. Zhang, F. Wu, J.-F. Chen, C. Xue and H. Zhao, *Phys. B*, 2017, 511, 10.
- H. Ren, B. Zhu, J. Zhu, Y. Hao, B. Yu and Y. Li, *Solid State Sci.*, 2011, 13, 938.
- G. Fadda, L. Colombo and G. Zanzotto, *Phys. Rev. B: Condens. Matter Mater. Phys.*, 2009, 79, 214102.
- K. C. Lau and B. I. Dunlap, *J. Phys.: Condens. Matter*, 2009, 21, 145402.
- A. Kuwabara, T. Tohei, T. Yamamoto and I. Tanaka, *Phys. Rev. B: Condens. Matter Mater. Phys.*, 2005, 71, 064301.
- M. Sternik and K. Parlinski, *J. Chem. Phys.*, 2005, 122, 064707.
- X. Zhao and D. Vanderbilt, *Phys. Rev. B: Condens. Matter Mater. Phys.*, 2002, 65, 075105.
- W. Wang, Z. Liang, X. Han, J. Chen, C. Xue and H. Zhao, *J. Alloys Compd.*, 2015, 622, 504.
- H. Wu, Y. Duan, K. Liu, D. Lv, L. Qin, L. Shi and G. Tang, *J. Alloys Compd.*, 2015, 645, 352.
- C. Carbogno, C. G. Levi, C. G. V. Walle and M. Scheffler, *Phys. Rev. B: Condens. Matter Mater. Phys.*, 2014, 90, 144109.
- J. E. Medvedeva, A. J. Freeman, C. B. Geller and D. M. Rishel, *Phys. Rev. B: Condens. Matter Mater. Phys.*, 2007, 76, 235115.
- Q.-J. Liu, Z.-T. Liu and L.-P. Feng, *Phys. B*, 2011, 406, 345.
- Y. Zhang, Y. Zhao, T. Otroshchenko, S. Han, H. Lund, U. Rodemerck, D. Linke, H. Jiao, G. Jiang and E. V. Kondratenko, *J. Catal.*, 2019, 371, 313.
- X. Wang, J. Zhao, W. Sun, Y. Pei, J. An, Z. Li and J. Rena, *Comput. Mater. Sci.*, 2019, 159, 210.
- F. Tran, J. Stelzl and P. Blaha, *J. Chem. Phys.*, 2016, 144, 204120.
- P. J. Hasnip, K. Refson, M. I. J. Probert, J. R. Yates, S. J. Clark and C. J. Pickard, *Philos. Trans. R. Soc., A*, 2014, 372, 20130270.
- G.-X. Zhang, A. M. Reilly, A. Tkatchenko and M. Scheffler, *New J. Phys.*, 2018, 20, 63020.
- L. Vega, J. Ruvireta, F. Vin˜es and F. Illas, *J. Chem. Theory Comput.*, 2018, 14, 395.
- Y. Hinuma, H. Hayashi, Y. Kumagai, I. Tanaka and F. Oba, *Phys. Rev. B*, 2017, 96, 094102.
- B. Himmetoglu, A. Floris, S. Gironcoli and M. Cococcioni, *Int. J. Quantum Chem.*, 2014, 114, 14.
- S. Grimme, A. Hansen, J. G. Brandenburg and C. Bannwarth, *Chem. Rev.*, 2016, 116, 5105.
- D. Mählberg, S. Sakong, K. F. Tonigold and A. Groß, *J. Chem. Theory Comput.*, 2019, 15, 3250.
- G. O. da Silva and J. B. L. Martins, *Comput. Theor. Chem.*, 2019, 1164, 112552.
- Y. Zhang and V. Ji, *Solid State Commun.*, 2012, 152, 1673.
- Y. Zhang, H.-X. Chen, L. Duana, J.-B. Fana, L. Nia, Z. Wanga, H. Lia and V. Jib, *Microelectron. Eng.*, 2019, 213, 77.
- Y. Zhang, Y. Zhao, T. Otroshchenko, H. Lund, M.-M. Pohl, U. Rodemerck, D. Linke, H. Jiao, G. Jiang and E. V. Kondratenko, *Nat. Commun.*, 2018, 9, 3794.
- S. Tosoni, H.-Y. T. Chen, A. R. Puigdollers and G. Pacchioni, *Philos. Trans. R. Soc., A*, 2017, 376, 20170056.
- S. C. Pandey, X. Xua, I. Williamson, E. B. Nelson and L. Li, *Chem. Phys. Lett.*, 2017, 669, 1.
- C. Ricca, A. Ringuède, M. Cassir, C. Adamo and F. Labat, *J. Comput. Chem.*, 2015, 36, 9.
- F. Gallino, C. Valentin and G. Pacchioni, *Phys. Chem. Chem. Phys.*, 2011, 13, 17667.
- D. W. Liu, C. H. Perry, A. A. Feinberg and R. Currat, *Phys. Rev. B: Condens. Matter Mater. Phys.*, 1987, 36, 9212.
- (a) J. P. Perdew, K. Burke and M. Ernzerhof, *Phys. Rev. Lett.*, 1996, 77, 3865; (b) J. P. Perdew and K. Burke, M.s Ernzerhof, *Phys. Rev. Lett.*, 1997, 78, 1396.
- J. P. Perdew, A. Ruzsinszky, G. I. Csonka, O. A. Vydrov, G. E. Scuseria, L. A. Constantin, X. Zhou and K. Burke, *Phys. Rev. Lett.*, 2008, 100, 136406.
- J. P. Perdew, A. Ruzsinszky, G. I. Csonka, O. A. Vydrov, G. E. Scuseria, L. A. Constantin, X. Zhou and K. Burke, *Phys. Rev. Lett.*, 2009, 102, 039902.
- B. Hammer, L. B. Hansen and J. K. Nørskov, *Phys. Rev. B: Condens. Matter Mater. Phys.*, 1999, 59, 7413.
- J. Tao, J. P. Perdew, V. N. Staroverov and G. E. Scuseria, *Phys. Rev. Lett.*, 2003, 91, 146401.
- S. Grimme, *J. Comput. Chem.*, 2006, 27, 1787.

- 49 S. Grimme, J. Antony, S. Ehrlich and H. Krieg, *J. Chem. Phys.*, 2010, 132, 154104.
- 50 A. Togo and I. Tanaka, *Scr. Mater.*, 2015, 108, 1.
- 51 V. I. Khitrova and V. V. Klechkovskaya, *Kristallografiya*, 1985, 30, 126.
- 52 J. E. Lowther, *Phys. Rev. B: Condens. Matter Mater. Phys.*, 2006, 73, 134110.
- 53 P. Haas, F. Tran, P. Blaha, L. S. Pedroza, A. J. R. da Silva, M. M. Odashima and K. Capelle, *Phys. Rev. B: Condens. Matter Mater. Phys.*, 2010, 81, 125136.
- 54 L. Lutterotti and P. Scardi, *J. Appl. Crystallogr.*, 1990, 23, 246.
- 55 S.-H. Guan, X.-J. Zhang and Z.-P. Liu, *J. Am. Chem. Soc.*, 2015, 137, 8010.
- 56 D. K. Smith and H. W. Newkirk, *Acta Crystallogr.*, 1965, 18, 983.
- 57 H. M. Kandil, J. D. Greiner and J. F. Smith, *J. Am. Ceram. Soc.*, 1984, 67, 341.
- 58 E. H. Kisi and C. J. Howard, *J. Am. Ceram. Soc.*, 1998, 81, 1682.
- 59 S.-K. Chan, Y. Fang, M. Grimsditch, Z. Li, M. V. Nevitt, W. M. Robertson and E. S. Zouboulis, *J. Am. Ceram. Soc.*, 1991, 74, 1742.
- 60 A. P. Mirgorodsky and P. E. Quintard, *J. Am. Ceram. Soc.*, 1999, 11, 3121.
- 61 G.-M. Rignanese, F. Detraux, X. Gonze and A. Pasquarello, *Phys. Rev. B: Condens. Matter Mater. Phys.*, 2001, 64, 134301.
- 62 R. H. French, S. J. Glass, F. S. Ohuchi, Y.-N. Xu and W. Y. Ching, *Phys. Rev. B: Condens. Matter Mater. Phys.*, 1994, 49, 5133.
- 63 M. T. Lanagan, J. K. Yamamoto, A. Bhalla and S. G. Sankar, *Mater. Lett.*, 1989, 7, 437.
- 64 A. Dwivedi and A. N. Cormack, *Philos. Mag.*, 1990, 61, 1.
- 65 J. C. Garcia, L. M. R. Scolfaro, A. T. Lino, V. N. Freire, G. A. Farias, C. C. Silva, H. W. L. Alves, S. C. P. Rodrigues and E. F. Silva, Jr, *J. Appl. Phys.*, 2006, 100, 104103.
- 66 G. Petretto, S. Dwaraknath, H. P. C. Miranda, D. Winston, M. Giantomassi, M. J. van Setten, X. Gonze, K. A. Persson, G. Hautier and G.-M. Rignanese, *Sci. Data*, 2018, 5, 180065.
- 67 A. P. Mirgorodsky, M. B. Smirnov and P. E. Quintard, *J. Phys. Chem. Solids*, 1999, 60, 985.